ARTICLE

Supporting Information for
Structure-based design and synthesis of copper (II) complexes as antivirus drug candidates targeting the SARS CoV-2 and HIV

Sunil Kumar[a], and Mukesh Choudhary[a]*

[a] *Department of Chemistry, National Institute of Technology Patna, Patna-800005 (Bihar) India.*

[a]. **Corresponding author: mukesh@nitp.ac.in*

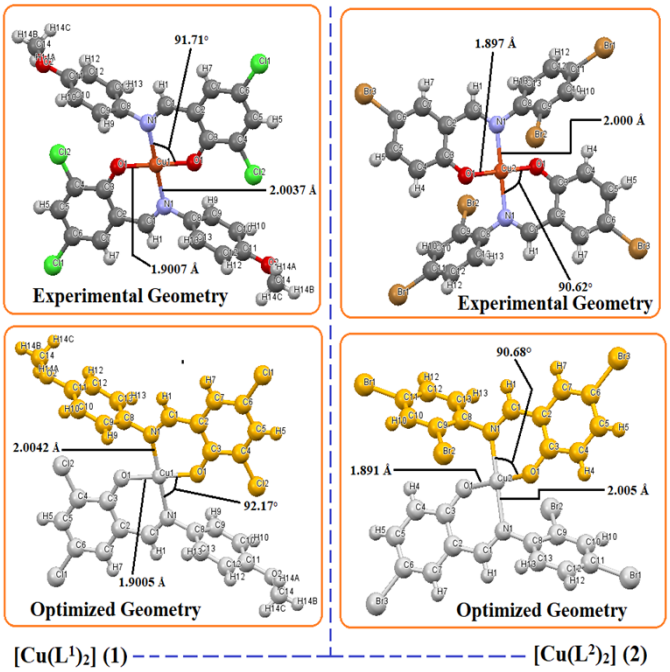

Figure S1. The experimental and quantum chemically optimized geometries of copper(II)complex $[Cu(L^1)_2]$(**1**) and $[Cu(L^2)_2]$(**2**).

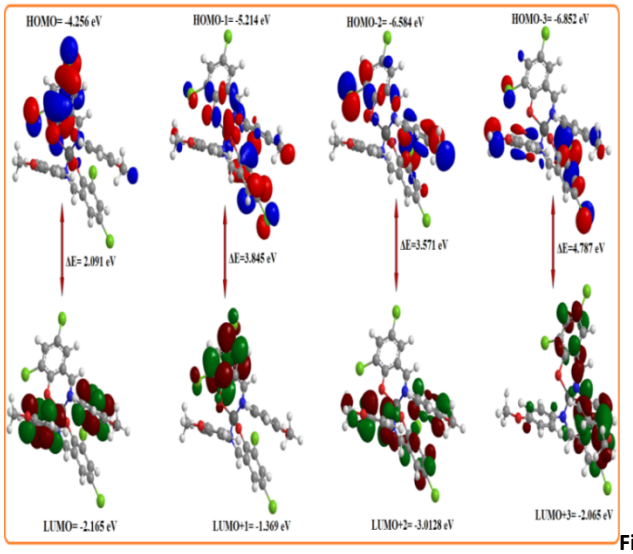

Figure S2. HOMO-LUMO energies and energy gap of copper (II) complex $[Cu(L^1)_2)]$(**1**).

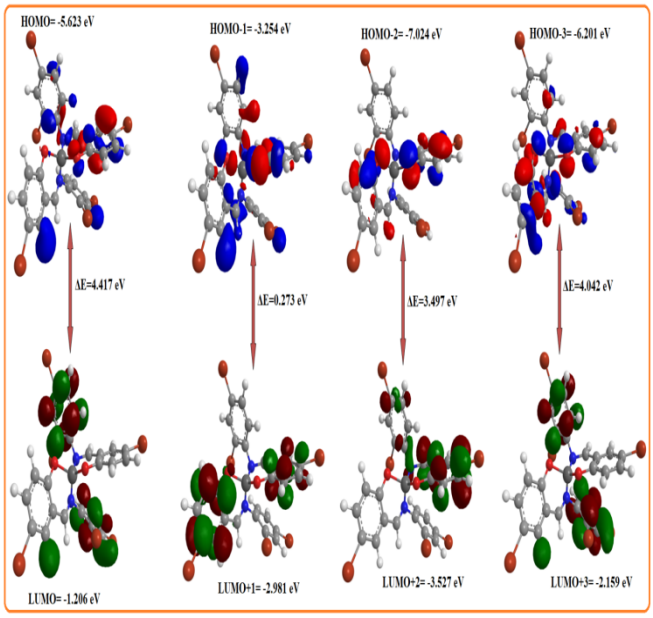

Figure S3. HOMO-LUMO energies and energy gap of copper (II) complex $[Cu(L^2)_2)]$(**2**).

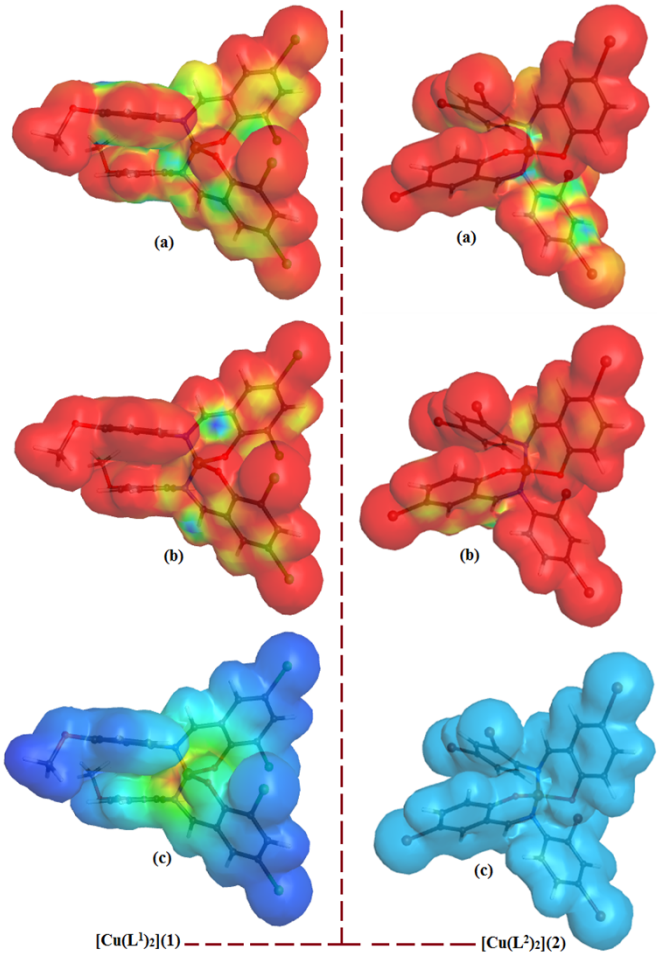

Figure S4. MEPs presentation including (a) radical frontier density, (b) electrophilic and nucleophilic frontier density (c) surface density for copper (II) complex $[Cu(L^1)_2)]$(**1**) and $[Cu(L^2)_2)]$(**2**).

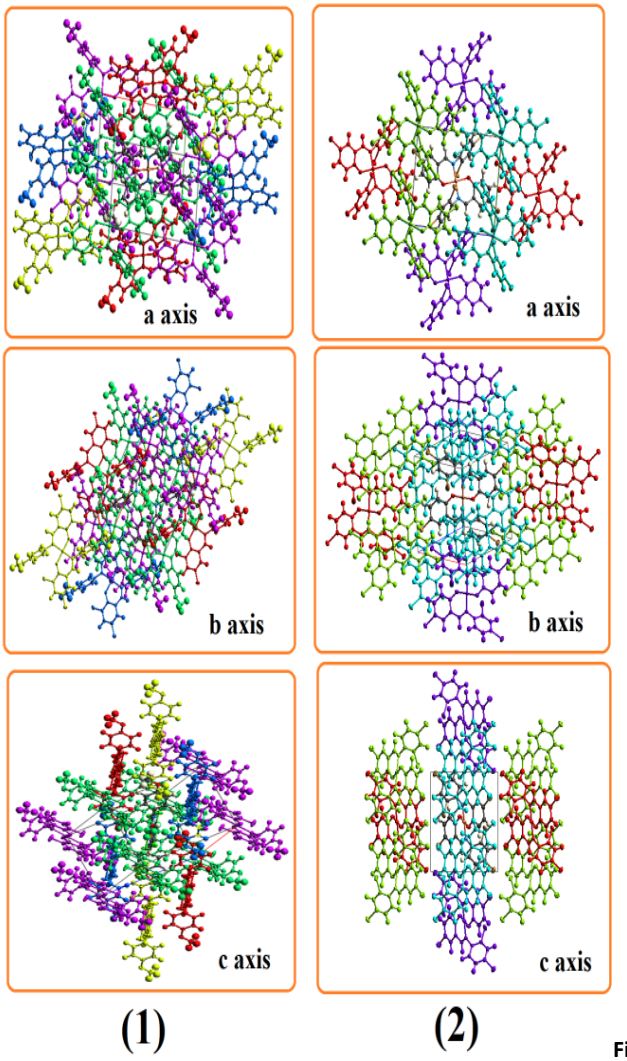

Figure S5. Packing cell diagrams mapped with energy framework for complex $[Cu(L^1)_2]$(**1**) and complex $[Cu(L^2)_2]$(**2**) viewed down the a-c axis.

$[Cu(L^1)_2)](1)$

	N	Symop	R	Electron Density	E_ele	E_pol	E_dis	E_rep	E_tot
	2	x, y, z	9.28	HF/3-21G	-9.0	0.0	-54.5	21.8	-40.6
	2	x, y, z	15.54	HF/3-21G	0.0	-1.9	0.0	0.0	-1.2
	4	-x+1/2, y+1/2, -z+1/2	8.42	HF/3-21G	-31.3	-8.0	-73.2	46.6	-65.2
	2	x, y, z	12.46	HF/3-21G	0.0	-1.6	0.0	0.0	-1.0
	4	-x+1/2, y+1/2, -z+1/2	11.39	HF/3-21G	-4.1	0.0	-14.2	3.7	-13.9

Energy Model	k_ele	k_pol	k_disp	k_rep
CE-HF ... HF/3-21G electron densities	1.019	0.651	0.901	0.811
CE-B3LYP ... B3LYP/6-31G(d,p) electron densities	1.057	0.740	0.871	0.618

$[Cu(L^2)_2](2)$

	N	Symop	R	Electron Density	E_ele	E_pol	E_dis	E_rep	E_tot
	2	x, y, z	14.14	HF/3-21G	0.0	-0.4	0.0	0.0	-0.3
	4	-x, y+1/2, -z+1/2	11.91	HF/3-21G	-6.2	-1.2	-31.4	24.6	-15.4
	4	-x, y+1/2, -z+1/2	8.35	HF/3-21G	-25.2	-5.9	-78.8	45.9	-63.3
	2	x, y, z	10.98	HF/3-21G	10.5	-4.4	-31.4	11.1	-11.5

Energy Model	k_ele	k_pol	k_disp	k_rep
CE-HF ... HF/3-21G electron densities	1.019	0.651	0.901	0.811
CE-B3LYP ... B3LYP/6-31G(d,p) electron densities	1.057	0.740	0.871	0.618

Figure S6 CE-B3LYP estimates of energy components and total energies (kJ/mol) for the closest intermolecular interactions in the complex $[Cu(L^1)_2]$(**1**) and complex $[Cu(L^2)_2]$(**2**).

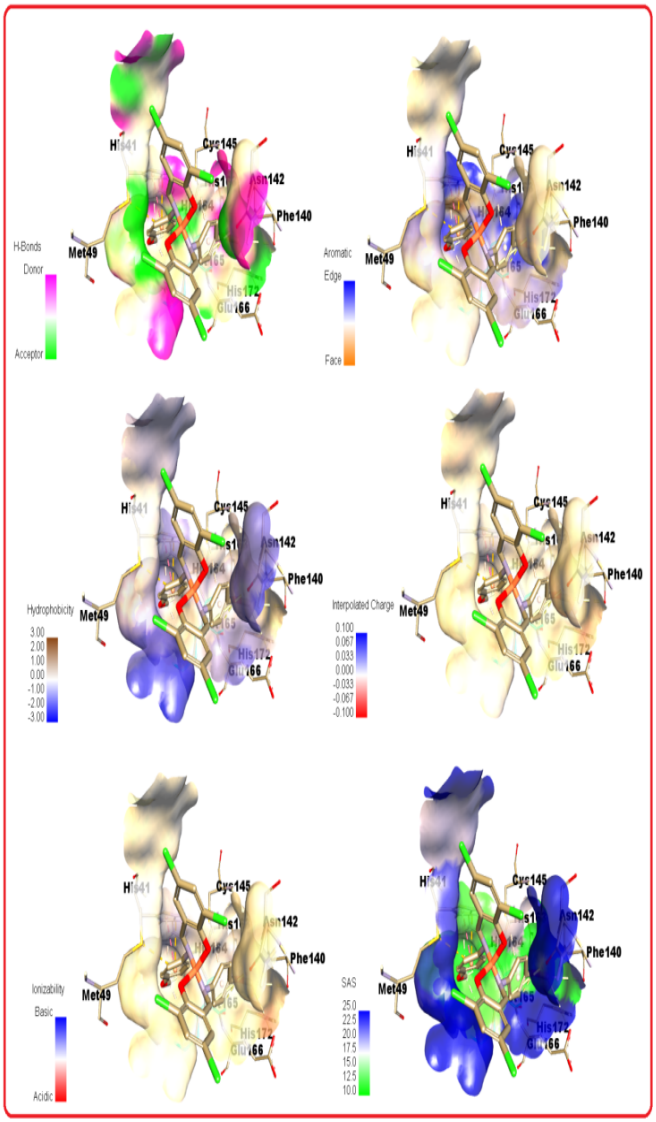

Figure S7. The representation of docked copper (II) complex $[Cu(L^1)_2)]$(**1**) with SARS-CoV-2 main protease for COVID-19 (PDB ID: 6XBG) (PDB ID: 6XBG) with an inhibitor UAW246 with its focused view for interacting residues along with H-bond and intermolecular interactions; (a) H-bond donor and acceptor meshes represented by pink and light green colours, respectively; (b) Aromatic receptor surface represented by blue (Edge) and light orange (face) colours; (c) Hydrophobic pocket represented with blue and brown colours; (d) interpolated charge receptor surface represented by blue and red colours; (e) ionizability receptor surface represented by blue (basic) and red (acidic) colours; (f) SAS receptor surface represented by blue and light green colours, respectively.

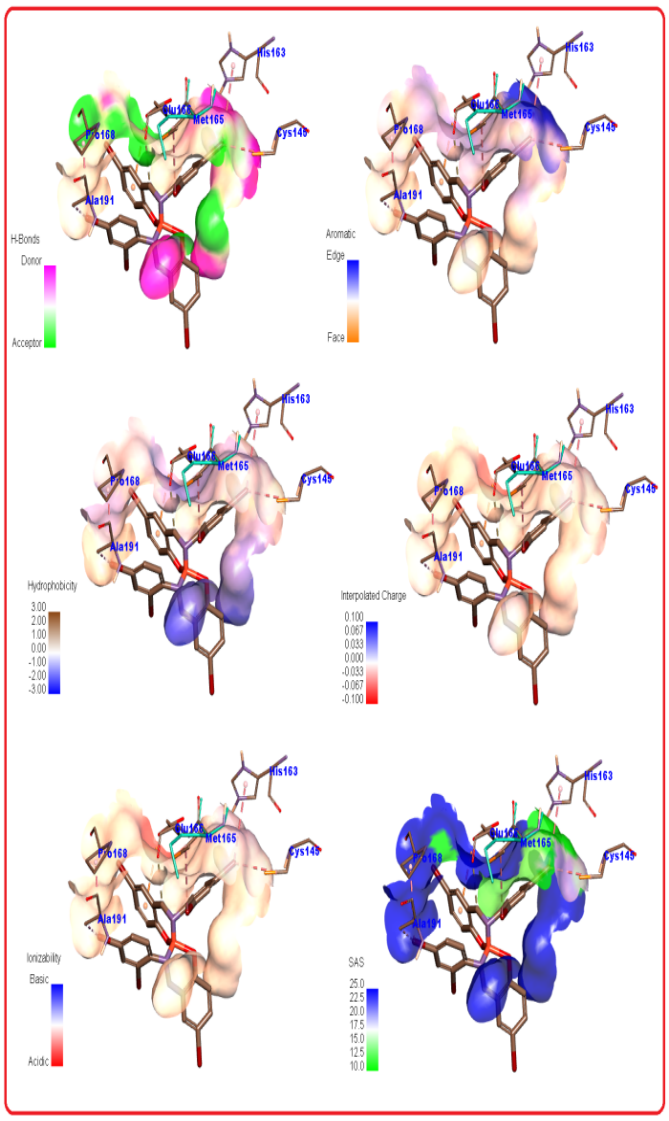

Figure S8. The representation of docked copper (II) complex $[Cu(L^2)_2)]$(**2**) with SARS-CoV-2 main protease for COVID-19 (PDB ID: 6XBG) (PDB ID: 6XBG) with an inhibitor UAW246 with its focused view for interacting residues along with H-bond and intermolecular interactions; (a) H-bond donor and acceptor meshes represented by pink and light green colours, respectively; (b) Aromatic receptor surface represented by blue (Edge) and light orange (face) colours; (c) Hydrophobic pocket represented with blue and brown colours; (d) interpolated charge receptor surface represented by light blue and light red colours; (e) ionizability receptor surface represented by light blue (basic) and light red (acidic) colours; (f) SAS receptor surface represented by blue and light green colours, respectively.

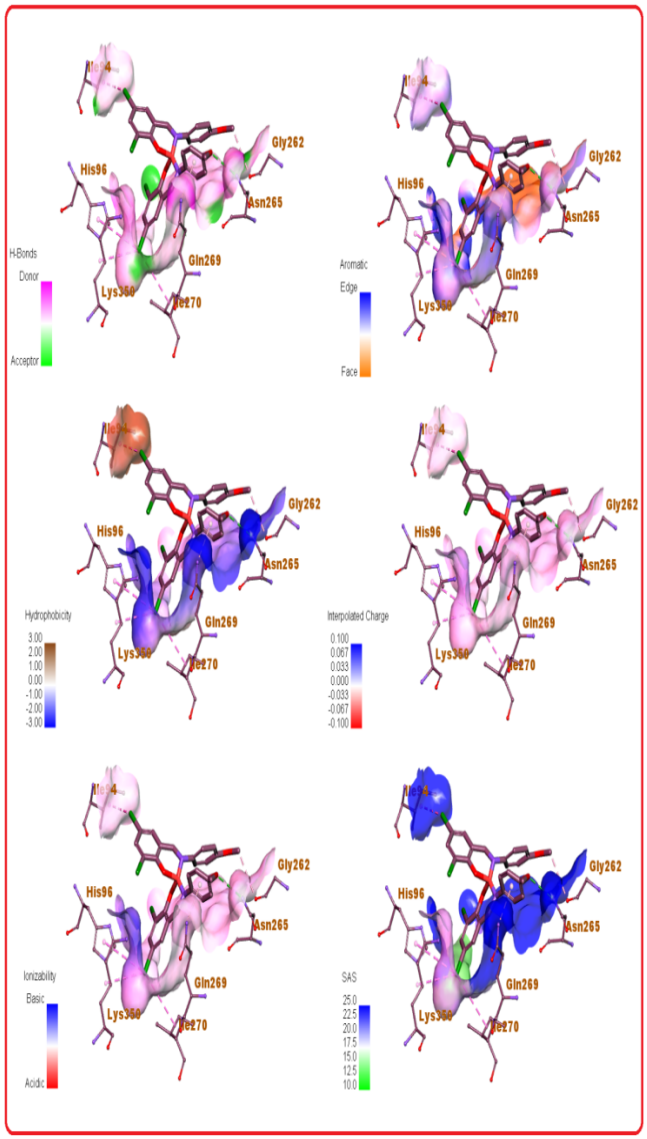

Figure S9. The representation of docked copper (II) complex $[Cu(L^1)_2)]$(**1**) inside the HIV-1 virus (PDB ID: 1JLE) with its focused view for interacting residues along with H-bond and intermolecular interactions; (a) H-bond donor and acceptor meshes represented by pink and light green colours, respectively; (b) Aromatic receptor surface represented by blue (Edge) and light orange (face) colours; (c) Hydrophobic pocket represented with blue and light brown colours; (d) interpolated charge receptor surface represented by pinkish blue and light red colours; (e) ionizability receptor surface represented by light blue (basic) and light red (acidic) colours; (f) SAS receptor surface represented by deep blue and light green colours, respectively.

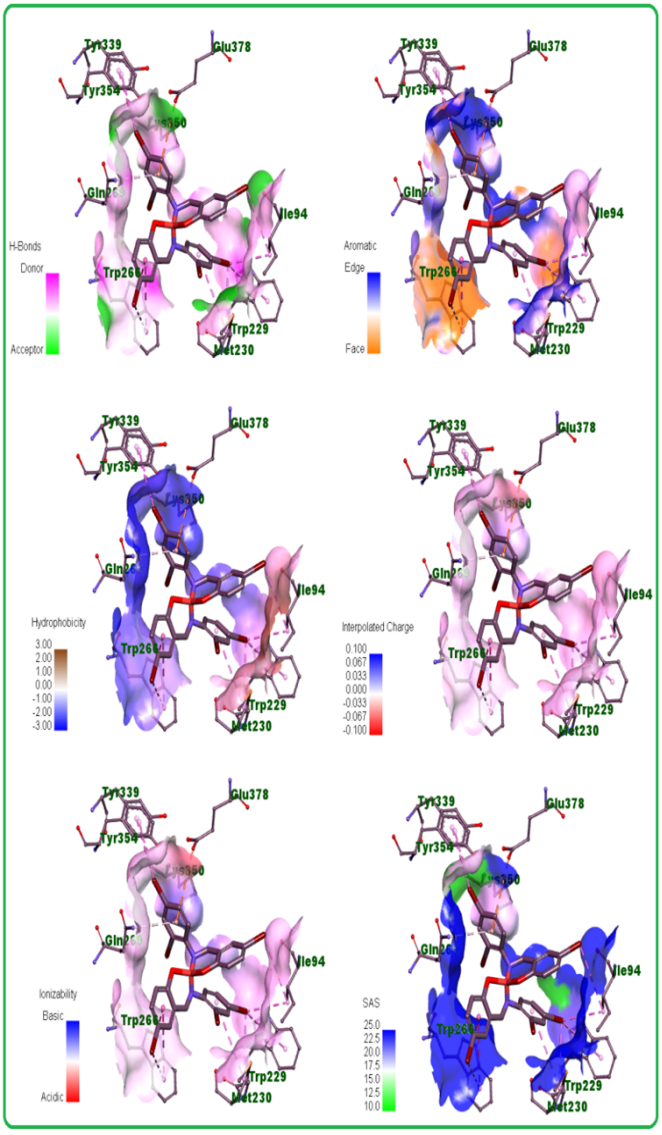

Figure S10. The representation of docked copper (II) complex $[Cu(L^2)_2)]$(**2**) inside the HIV-1 virus (PDB ID: 1JLE) with its focused view for interacting residues along with H-bond and intermolecular interactions; (a) H-bond donor and acceptor meshes represented by pink and light green colors, respectively; (b) Aromatic receptor surface represented by blue (Edge) and light orange (face) colors; (c) Hydrophobic pocket represented with blue and light brown colors; (d) interpolated charge receptor surface represented by light blue and light red colors; (e) ionizability receptor surface represented by light blue (basic) and light red (acidic) colors; (f) SAS receptor surface represented by deep blue and light green colors, respectively.

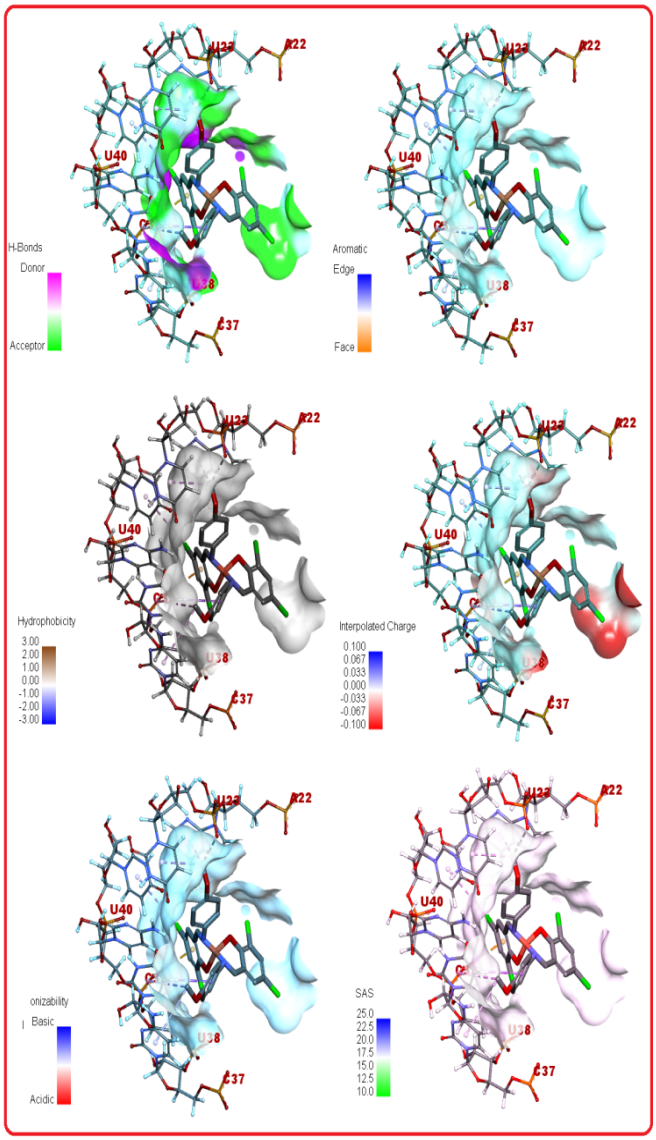

Figure S11. The representation of docked copper (II) complex $[Cu(L^1)_2)]$(**1**) inside the HIV-1 RNA virus (PDB ID: 1UUD) with its focused view for interacting residues along with H-bond and intermolecular interactions; (a) H-bond donor and acceptor meshes represented by pink and light green colours, respectively; (b) Aromatic receptor surface represented by cyanic blue (Edge) and light orange (face) colours; (c) Hydrophobic pocket represented with light blue and brown colours; (d) interpolated charge receptor surface represented by blue and red colours; (e) ionizability receptor surface represented by blue (basic) and red (acidic) colours; (f) SAS receptor surface represented by blue and light green colours, respectively.

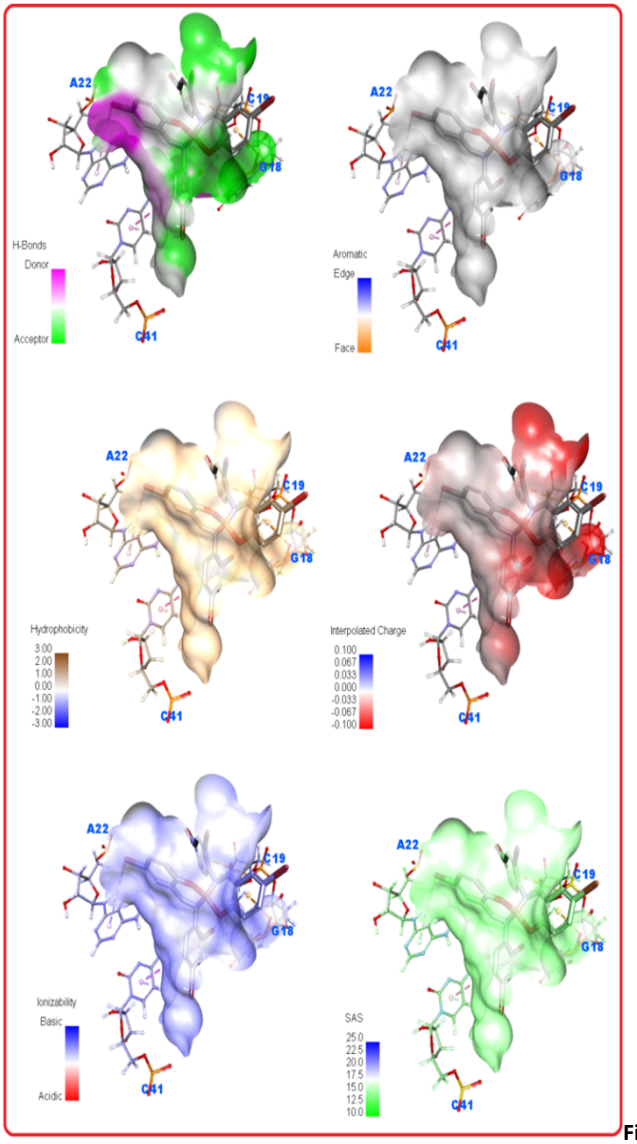

Figure S12. The representation of docked copper (II) complex $[Cu(L^2)_2)]$(**2**) inside the HIV-1 RNA virus (PDB ID: 1UUD) with its focused view for interacting residues along with H-bond and intermolecular interactions; (a) H-bond donor and acceptor meshes represented by pink and light green colours, respectively; (b) Aromatic receptor surface represented by blue (Edge) and orange (face) colours; (c) Hydrophobic pocket represented with light blue and light brown colours; (d) interpolated charge receptor surface represented by light blue and red colours; (e) ionizability receptor surface represented by light blue (basic) and red (acidic) colours; (f) SAS receptor surface represented by blue and light green colours, respectively.

Table S1. Experimental and optimized values of the studied complex copper complex $[Cu(L^1)_2]$(**1**) and $[Cu(L^2)_2]$(**2**)].

Complexes	Experimental bond lengths (Å)		Theoretical bond lengths (Å)	
(**1**)	Cu(1)-O(1) Cu(1)-N(1) Cl(1)-C(6) Cl(2)-C(4)	1.9007 2.0037 1.7395 1.7207	Cu(1)-O(1) Cu(1)-N(1) Cl(1)-C(6) Cl(2)-C(4)	1.9005 2.0042 1.7394 1.7209
(**2**)	Cu(2)-O(1) Cu(2)-N(1) Br(3)-C(6) Br(2)-C(9)	1.897 2.000 1.898 1.889	Cu(2)-O(1) Cu(2)-N(1) Br(3)-C(6) Br(2)-C(9)	1.891 2.005 1.897 1.890

Table S2. The structure activity relationship established between the structures of the copper complex $[Cu(L^1)_2]$(**1**) and $[Cu(L^2)_2]$ (**2**) and their potential applications against SARS-CoV-2 main protease (M^{pro}) and HIV inhibitors.

Complexes		Experimental bond lengths (Å)		Docked complex inside SARS-CoV-2 bond lengths (Å)		Docked complex inside HIV-1 bond lengths (Å)	
(**1**)	6XBG	Cu(1)-O(1) Cu(1)-N(1) Cl(1)-C(6) Cl(2)-C(4)	1.9007 2.0037 1.7395 1.7207	Cu(1)-O(1) Cu(1)-N(1) Cl(1)-C(6) Cl(2)-C(4)	1.9015 2.0027 1.7389 1.7219	Cu(1)-O(1) Cu(1)-N(1) Cl(1)-C(6) Cl(2)-C(4)	1.9018 2.0034 1.7387 1.7213
	1JLE	Cu(1)-O(1) Cu(1)-N(1) Cl(1)-C(6) Cl(2)-C(4)	1.9007 2.0037 1.7395 1.7207	Cu(1)-O(1) Cu(1)-N(1) Cl(1)-C(6) Cl(2)-C(4)	1.9013 2.0032 1.7384 1.7215	Cu(1)-O(1) Cu(1)-N(1) Cl(1)-C(6) Cl(2)-C(4)	1.9011 2.0044 1.7405 1.7213
	1UUD	Cu(1)-O(1) Cu(1)-N(1) Cl(1)-C(6) Cl(2)-C(4)	1.9007 2.0037 1.7395 1.7207	Cu(1)-O(1) Cu(1)-N(1) Cl(1)-C(6) Cl(2)-C(4)	1.9021 2.0029 1.7388 1.7216	Cu(1)-O(1) Cu(1)-N(1) Cl(1)-C(6) Cl(2)-C(4)	1.9012 2.0049 1.7409 1.7211
(**2**)	6XBG	Cu(2)-O(1) Cu(2)-N(1) Br(3)-C(6) Br(2)-C(9)	1.897 2.000 1.898 1.889	Cu(2)-O(1) Cu(2)-N(1) Br(3)-C(6) Br(2)-C(9)	1.889 2.008 1.891 1.894	Cu(2)-O(1) Cu(2)-N(1) Br(3)-C(6) Br(2)-C(9)	1.896 2.006 1.896 1.897
	1JLE	Cu(2)-O(1) Cu(2)-N(1) Br(3)-C(6) Br(2)-C(9)	1.897 2.000 1.898 1.889	Cu(2)-O(1) Cu(2)-N(1) Br(3)-C(6) Br(2)-C(9)	1.898 2.007 1.887 1.891	Cu(2)-O(1) Cu(2)-N(1) Br(3)-C(6) Br(2)-C(9)	1.891 2.004 1.902 1.887
	1UUD	Cu(2)-O(1) Cu(2)-N(1) Br(3)-C(6) Br(2)-C(9)	1.897 2.000 1.898 1.889	Cu(2)-O(1) Cu(2)-N(1) Br(3)-C(6) Br(2)-C(9)	1.902 2.005 1.896 1.893	Cu(2)-O(1) Cu(2)-N(1) Br(3)-C(6) Br(2)-C(9)	1.898 2.003 1.894 1.908

ARTICLE